Nonequilibrium capillarity effects in two-phase flow through porous media at different scales

S. Bottero,[1,2] S. M. Hassanizadeh,[2] P. J. Kleingeld,[2] and T. J. Heimovaara[3]

Received 9 May 2011; revised 13 July 2011; accepted 28 July 2011; published 8 October 2011.

[1] A series of primary drainage experiments was carried out in order to investigate nonequilibrium capillarity effects in two-phase flow through porous media. Experiments were performed with tetrachloroethylene (PCE) and water as immiscible fluids in a sand column 21 cm long. Four drainage experiments were performed by applying large pressures on the nonwetting phase at the inlet boundary: 20, 30, 35, 38 kPa. Our results showed that the nonequilibrium local fluids pressure difference-saturation curves are above the capillary pressure saturation curve. Moreover, the nonequilibrium pressure difference showed a nonmonotonic behavior with an overshoot that was more pronounced at higher injection pressures. The dynamic capillarity coefficient τ was calculated from measured local pressures and saturations (the scale of sensor devices, 0.7 cm). Its value was found to vary between 1.3×10^5 to 2×10^5 Pa s. Within the saturation range of $0.50 > S_w > 0.85$, no clear dependency of the dynamic coefficient on the wetting saturation was observed. Also, no dependency of the dynamic capillarity coefficient on the applied boundary pressure was found. Averaged values of $[\tau]$ at the length scales of 11 and 18 cm were also estimated from averaged pressures and saturations. The upscaled dynamic coefficient was found to vary between 0.5×10^6 and 1.2×10^6 Pa s at the average window size of 11 cm. This is one order of magnitude larger than the local-scale coefficient. Larger values were found for the length scale of 18 cm: 1.5×10^6 and 2.5×10^6 Pa s. This suggests that the value of dynamic coefficient increases with the scale of observation.

Citation: Bottero, S., S. M. Hassanizadeh, P. J. Kleingeld, and T. J. Heimovaara (2011), Nonequilibrium capillarity effects in two-phase flow through porous media at different scales, *Water Resour. Res., 47*, W10505, doi:10.1029/2011WR010887.

1. Introduction

[2] Two-phase flow processes are usually modeled by the mass balance equation and Darcy's equation for each phase. When combined, they result in the following equation [*Bear*, 1972; *Helmig*, 1997]:

$$\phi \frac{\partial S_\alpha}{\partial t} = \nabla \cdot \left[\frac{k_{r\alpha}(S_\alpha)}{\mu_\alpha} \mathbf{k} \cdot (\nabla P_\alpha - \rho_\alpha \mathbf{g}) \right]; \quad \alpha = w, n \qquad (1)$$

where ϕ denotes porosity, S is the saturation, k_r is the relative permeability, $\mathbf{k}$ is the intrinsic permeability, μ denotes the dynamic viscosity, $\mathbf{g}$ is the gravity acceleration, ρ indicates the density, and ∇P is the pressure gradient. The subscripts w and n denote wetting and nonwetting phases, respectively. All quantities appearing in these two equations are macroscale quantities. Assuming that porosity, relative permeability, and fluids properties are known, and considering that $S_w + S_n = 1$, the unknowns in this set of equations are: P_n, P_w, and S_w. Obviously, we are short of one equation. Commonly this deficit is eliminated by an equation which states that the pressure difference between the two phases is a function of wetting phase saturation:

$$P_n - P_w = f(S_w). \qquad (2)$$

This is also known as "the capillary-pressure saturation relationship" because in the literature, the fluids pressure difference is commonly assumed to be the macroscale "capillary pressure" P_c. Thus, one commonly writes:

$$P_n - P_w = P_c(S_w). \qquad (3)$$

This expression is a source of some of the misunderstandings associated with two-phase flow theory. In fact, the macroscale pressure difference $P_n - P_w$ is not the same as capillary pressure P_c. This holds even at the pore scale where the capillary pressure originally is defined. The capillary pressure is an intrinsic property of the porous medium and the two fluids. For a meniscus, it is defined, independently of the fluid pressures, by the Young-Laplace equation:

$$p_c = \sigma \left(\frac{1}{r_1} + \frac{1}{r_2} \right) = \frac{2\sigma}{R_m}, \qquad (4)$$

where σ represents the fluid–fluid interfacial tension, r_1 and r_2 denote the principal radii of curvature of the meniscus, and R_m is the mean radius of curvature. Thus, through r_1 and

[1]Department of Biotechnology, Delft University of Technology, Delft, Netherlands.
[2]Department of Earth Sciences, Utrecht University, Utrecht, Netherlands.
[3]Geo-Engineering Section, Delft University of Technology, Delft, Netherlands.

0043-1397/11/2011WR010887

r_2 the capillary pressure depends on the pore dimension and through the interfacial tension it depends on the interfacial properties of the fluids and the porous solid. Equation (4) is assumed to be valid whether the interface is moving or not. The relationship between $p_n - p_w$ and p_c in a pore, however, depends on flow conditions. This relationship can be derived from the force balance in the direction normal to the interface. In this respect, *Hassanizadeh and Gray* [1993] derived the following force balance equation in the direction N normal to an interface:

$$p_n - p_w = \frac{2\sigma}{R_m} + \mathbf{N} \cdot (\tau_n - \tau_w) \cdot \mathbf{N} - (\nabla^\sigma \cdot \tau_{wn}) \cdot \mathbf{N}, \qquad (5)$$

where p_n and p_w are microscale pressures of the two fluids on two sides of the meniscus, τ_n and τ_w are their corresponding viscous stress tensors, and τ_{wn} is the interfacial viscous stress tensor. It is evident that in such a case $p_n - p_w$ is not equal to $p_c = \frac{2\sigma}{R_m}$. Even if interfacial viscous forces (last term in equation (5)) are negligible or not present at all, $p_n - p_w$ may still be different form p_c because of dissipative forces within the fluids surrounding the meniscus. The significance of the effect of these forces has been shown, for instance, by *Sheng and Zhou* [1992], who have studied the motion of a meniscus in a tube during piston displacement of a wetting phase by a nonwetting phase or vice versa. They found:

$$p_n - p_w = p_c \pm B\left(\frac{\mu q}{r}\right)^A, \qquad (6)$$

where p_n and p_w are pressures on the two sides of the interface, μ is viscosity, q is fluid velocity through the tube, and B and A are coefficients that control the velocity-dependent "capillary pressure." Thus, the relationship $p_n - p_w = p_c$ is valid at the meniscus under static conditions only. Under dynamic conditions, $p_n - p_w$ depends on the flow velocity.

[3] Even if the pore scale nonequilibrium term in equation (6) is negligible, so that we have $p_n - p_w = p_c$ at all menisci within a representative elementary volume (REV) under flow conditions, it does not mean that the same can be said at macroscale. Obviously, since fluid pressures are spatially variable within each flowing phase, macroscale (or average) pressure values will be different from pressure values at the interface. This has been shown by *Dahle et al.* [2005] through a calculation of average pressures in a bundle of tubes model. In fact, on the basis of thermodynamic considerations, *Hassanizadeh and Gray* [1990] and *Kalaydjian* [1992] derived an equation which relates the difference in the macroscale fluids pressure, $P_n - P_w$, to the macroscale capillary pressure P_c and the rate change of saturation. A linear approximation is given as

$$P_n - P_w = P_c(S_w) - \tau(S_w)\frac{\partial S_w}{\partial t}, \qquad (7)$$

where τ is a dynamic capillarity coefficient, also called a damping coefficient. In this formulation, P_c is an intrinsic property of the porous medium-fluids system, whereas fluids pressure difference $P_n - P_w$ is dependent on flow dynamics (and thus initial and boundary conditions). In the literature, the terms "static capillary pressure" (referring to P_c) and "dynamic capillary pressure" (referring to, $P_n - P_w$), have been used. This is potentially confusing terminology; in fact, there is only one capillary pressure, as explained above. So, we propose to refer to $P_n - P_w$ as nonequilibrium *fluids pressure difference* or simply as *pressure difference*. $P_c(S_w)$ denotes the capillary pressure which is measured experimentally as a function of saturation in equilibrium experiments. Obviously, the pressure difference between the wetting and nonwetting phase is equal to capillary pressure only under equilibrium conditions. In fact, equation (7) suggests that when the equilibrium is disturbed, the saturation will change to re-establish the equilibrium condition, and the coefficient τ controls this process.

[4] Most nonequilibrium experiments reported in the literature deal with unsaturated flow [*Topp et al.*, 1967; *Smiles et al.*, 1971; *Vachaud et al.*, 1972; *Stauffer*, 1978; *Wildenschild et al.*, 2001; *Chen*, 2006; *Sakaki et al.*, 2010; *Camps-Roach et al.*, 2010]. A comprehensive review of nonequilibrium laboratory experiments was given by *Hassanizadeh et al.* [2002]. A review of computational models is found in the work of *Joekar-Niasar and Hassanizadeh* [2011]. Only a few nonequilibrium experiments have involved two phases, such as oil and water [*Kalaydjian*, 1992; *Hassanizadeh et al.*, 2004; *O'Carroll et al.*, 2005]. In this work, we performed a series of nonequilibrium drainage experiments, in order to investigate the nonequilibrium capillarity effect in two-phase flow involving water and PCE. Nonequilibrium primary drainage experiments were carried out in a homogeneous sand column with a range of (large) injection pressure values. Experimental results are presented and compared with equilibrium experimental data. First, local-scale values of the damping coefficient were calculated on the basis of locally measured values of pressures and saturations. Next, column-scale values of τ were calculated on the basis of average pressures and saturation values. The results are compared to determine scale dependence of the dynamic coefficient.

2. Materials and Methods

2.1. Experimental Set-up

[5] Tetrachloroethylene (PCE) and de-mineralized, deaired water were used as the nonwetting and wetting phases, respectively. Physical properties of the two fluids are presented in Table 1. In order to visualize the displacement of one phase by the other, PCE was colored with Sudan-Red dye (with a concentration of 1.3 mg L^{-1}).

[6] A schematic representation of the experimental setup is shown in Figure 1. Details of the experimental setup and procedure can be found in the work of *Bottero* [2009] and *Bottero et al.* [2011]. It consists of a column 21 cm high with an inner diameter of 9.83 cm, connected to inflow and outflow burettes, each 120 cm high and 4.95 cm in inner diameter. We used plexiglas for both the column and

Table 1. Fluid Properties

Properties	Water	PCE	Unit
Density	1000	1623	(kg m^{-3})
Viscosity	1×10^{-3}	0.9×10^{-3}	(Pa s)

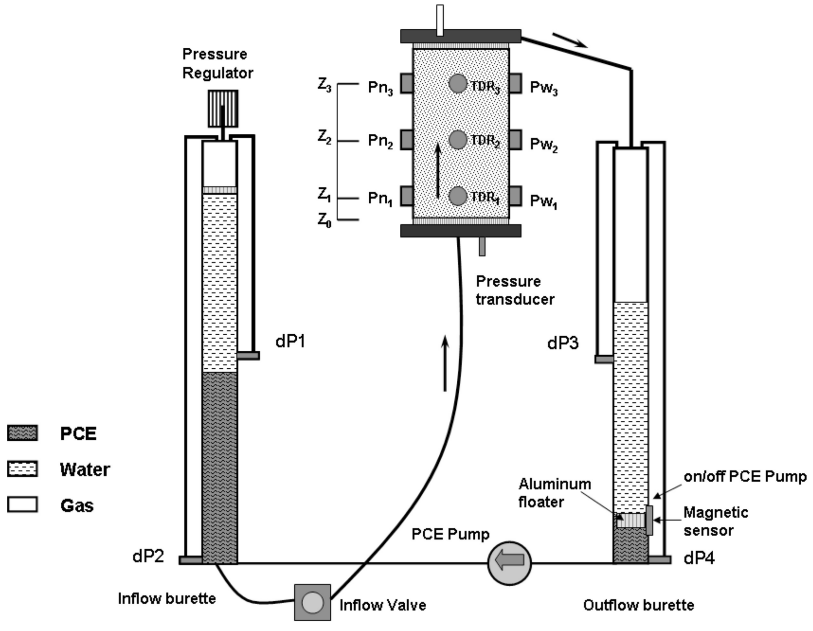

Figure 1. Experimental setup (not to scale).

burettes. Viton o-rings were used at joints to avoid any leakage. Two stainless-steel porous plates (mean pore size, 40 μm; thickness, 3 mm), one at the base and one at the top of the column, kept the sand in place. A distribution plate was placed under the bottom porous plate to guarantee uniform inflow of the invading fluid. This was ensured by engraving in the plate circumferential and radial channels (0.5–1.0 cm wide and 0.3–0.6 cm deep).

[7] In order to keep a desired constant nonwetting phase pressure at the bottom of the column, a control-pressure system was designed. It consisted of a pressure transducer installed just below the distribution plate and a pressure regulator (Proportion-Air, BB1, electro-pneumatic pressure control valve) placed at the top of the inflow burette. The pressure transducer monitored the pressure of the inflowing fluid at the bottom of the column while the pressure regulator regulated the pressure of the gas phase inside the inflow burette. An algorithm was written to control both pressure regulator and pressure transducer. In this way, any pressure change at the bottom of the column was rapidly and automatically compensated by pressure change in the gas phase, restoring the bottom pressure to a preset value. The outflow on top of the column was kept at constant atmospheric pressure. This was achieved through a small opening (0.5 cm diameter) that was connected to a balloon filled with Argon gas. This prevented evaporation of water or volatilization of PCE.

[8] The water and PCE pressures at various elevations in the column were measured by means of selective pore pressure transducers. Standard pressure transducers (Kulite XTM190) were modified and were made either hydrophobic or hydrophilic by means of hydrophobic and hydrophilic filters (Porex PE Sintered; pore size, 150 μm, thickness, 5 mm) and membranes (Durapore PVDF/HVHP and Durapore PVDF/HVLP; mean pore size, 0.45 μm, thickness, 125 μm). A sensor case was designed to hold the membrane, filter, and pressure transducer. During the experiment, the membrane was in direct contact with the sand while the filter served to support the membrane. An important requirement for the proper functioning of the selective pressure sensor was to avoid the presence of air. This was ensured by putting filters, membranes, and sensor cases in the corresponding fluids, i.e., water for the wetting phase and silicon oil for the nonwetting phase, and de-airing by applying a vacuum for 12 h. The assembling of various parts of a selective pressure transducer was done inside the corresponding fluids avoiding any contact of filters and membranes with air. A full description of the transducers and their preparation can be found in the work of *Oung and Bezuijen* [2003] and *Bottero* [2009].

[9] Three pairs of selective pore pressure transducers were installed at three different elevations $z_1 = 7$ cm, $z_2 = 12.5$ cm, and $z_3 = 18$ cm (see Figure 1). Each pair consisted of a wetting phase and a nonwetting phase transducer inserted at the opposite sides of the column. The face opening of the transducer in contact with soil had a diameter of 7 mm. Moreover, it was flush with the inner wall of the plexiglas column, so that the transducers did not protrude into the soil. The transducers at elevation z_i were designated by Pw_i and Pn_i for the wetting and nonwetting phases, respectively. All pressure sensors were connected to a 24-channel data logger (Hewlett Packard 3497A).

[10] The local water saturation was measured inside the sand column using three time domain reflectometry (TDR) probes, placed at the same three elevations as the pore pressure transducers. Each TDR probe had two prongs, positioned in a horizontal plane with 1 cm spacing. Thus, the measurement window of a TDR had almost the same size as a pressure transducer. TDRs were connected by 1-m long coaxial cables of 50 Ω to a time domain reflectometry measuring device, TDR100 (Campbell Scientific Inc.), via coaxial multiplexer units SDMX50 (Campbell Scientific Inc). An algorithm was written in MATLAB (http://

www.mathworks.com) to control the multiplexer and to acquire the saturation as a function of time.

[11] Preliminary tests were performed to verify the time response of nonwetting and wetting pressure transducers. The pressure device was installed inside a test column filled with water. The pressure in the inlet burette was increased by the pressure regulator and only when a preset pressure was reached at the bottom of the column, the valve was opened allowing fluid flow upward. The transducers responded to the pressure change within a time span of 0.3 s. The response of the time domain reflectometry was tested by submerging and then removing the TDR prongs in water. These sensors responded to the water content change in less than 0.5 s.

[12] The average (column-scale) fluid saturation over the whole sand column was determined from the change of volumes of fluids in inflow and outflow burettes. This volume change was measured through changes in fluid pressures in the burettes. For this purpose, four differential pressure transducers (PDCR-4160) were used (see Figure 1), two placed in the inflow burette (dP_1 and dP_2) and two in the outflow burette (dP_3 and dP_4). The differential pressures measured the change of pressure head of the two immiscible fluids. As there was no evaporation of water and/or volatilization of PCE, the volume change of a fluid in the two burettes could only be due to the change of its volume inside the sand column.

[13] Contrary to many two-phase flow column experiments, no hydrophilic and/or hydrophobic membranes were used at the column inlet/outlet in our setup. Such membranes can affect the distribution of fluids in the sand column. Therefore, during drainage experiments, when the PCE breakthrough occurred, a large volume of the wetting phase was still present in the column. To reduce the volume of the wetting phase in the sand column, the outflow of both PCE and water was continued until steady state flow of the nonwetting phase was reached. At steady state, there was no flow of water, but, continuous flow of PCE at a constant rate. Thus, a large volume of PCE had to flow through the column. In order to reduce the volume of PCE that was needed, a recirculation system was devised consisting of the two burettes, a gear PCE pump, and an on/off switch that controlled the PCE pump. A switch consisted of one magnetic sensor, which was activated and deactivated when coming into contact with an aluminum floater inside the outflow burette (see Figure 1). The floater and the magnetic sensor were placed in the lower side of the outflow burette to control the on/off switch of the PCE pump throughout the drainage processes. During nonequilibrium drainage experiments, the nonwetting fluid from the inflow burette was injected into the bottom of the column to avoid any instability due to gravity. After exceeding its entry pressure, PCE flowed upward in the sand column, displacing water. The outflowing water and later the outflowing PCE were collected in the outflow burette. Due to its higher density, the PCE sank to the bottom of the burette and was pumped back into the inflowing burette for continuous recirculation. In the inflow burette, a floater was placed on the surface of water to prevent contact between water and gas phases and therefore reduce the possibility of dissolution of air in water.

[14] All experiments were carried out in a constant-temperature room at 20 ± 0.5°C.

2.2. Sand Column Preparation

[15] The sand used in all experiments was a natural Dutch sand called Zijenzand. It was first sieved to obtain a grain size distribution with $D_{15} = 0.06$ mm and $D_{60} = 0.09$ mm. It was then washed in order to flush away fine clay particles. Finally, it was dried in an oven at 105°C for 24 h. The top and bottom porous plates were cleaned in an alcohol bath for 40 min to remove any impurity, and then in an ultrasonic bath filled with water for another 40 min to remove fine particles which could clog the pore space. Demineralized, deaired water was used in all operations and experiments. The bottom porous plate was mounted on the inflow distribution plate together with the plexiglass column and sealed with viton o-ring to avoid leakage. Pressure transducer, selective pressure transducers and TDR's were then mounted. The column was subsequently filled with de-aired, demineralized water. During this step, care was taken to avoid the contact of selective pressure transducers with air. Therefore, the water level inside the column was gradually increased and only when it reached a specific elevation, the corresponding transducer was mounted. The sand packing inside the column was done continuously, pouring dry sand into water and tapping the column at the same time. Before pouring the next layer, the sand in the column was gently mixed with a comb (attached to a long handle) to avoid layering. Our results showed that this procedure produced a reasonably homogeneous sand packing. The column was repacked for each experiment.

[16] Calibration of the TDR was based on the refractive mixing model for three phases (sand, water, and PCE) [*Schaap et al.*, 1997; *Malicki et al.*, 1994]. Wetting phase transducers were calibrated to measure hydrostatic pressure before the start of the primary drainage, whereas, nonwetting phase pressure transducers were calibrated to measure oil static pressure at the end of the drainage experiment after the flow was stopped. In preliminary tests, we established that no pressure drift occurred in the time frame that the experiments were performed.

3. Nonequilibrium Experiments

3.1. Procedure

[17] In this paper, only nonequilibrium experiments will be shown and discussed. Equilibrium two-phase experiments for the same fluids-porous media system are presented by *Bottero et al.* [2011], where both local- and column-scale capillary pressure saturation curves are given. A nonequilibrium primary drainage experiment was started by applying large pressure to the inflowing PCE and keeping it constant throughout the experiment. The column was initially fully water-saturated and PCE was injected from below. Experiments were carried out at four different injection pressures: 20, 30, 35, and 38 kPa. Local fluid pressures, local water saturation, as well as the average saturation were recorded every 3 s for 15 h.

3.2. Results and Discussions

[18] Plots of measured fluid pressures as a function of time for the four different injection pressures are shown in Figures 2a, 2d, 3a, and 3d. Only pressure values at early times are shown here. This is because the nonequilibrium effect plays a role mainly at the early time of the drainage

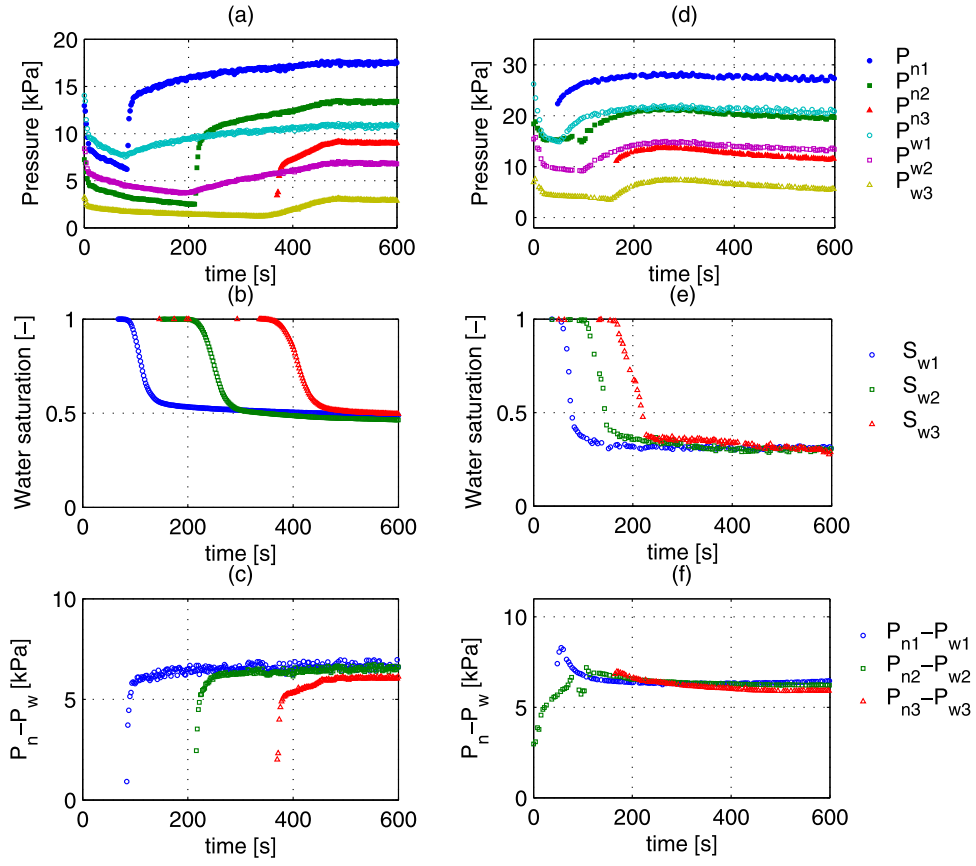

Figure 2. Results of nonequilibrium experiments at three different elevations. Figures on left are at an injection pressure of 20 kPa and right figures are at an injection pressure of 30 kPa. (a) and (d) Wetting and nonwetting phase pressures versus time. (b) and (e) Local water saturation versus time. (c) and (f) Local fluids pressure difference versus time.

process when a large change in saturation and pressure occurred. A general trend can be noticed in all experiments. We can distinguish four main stages:

[19] 1. As soon as the inflow valve (see Figure 1) was opened, all pressure transducers registered a high value depending on the injection pressure.

[20] 2. As the nonwetting phase flowed into the column displacing the wetting phase, pressure of both fluids dropped sharply until the front of the nonwetting phase arrived at a given set of transducers.

[21] 3. As soon as the PCE front reached a pair of transducers, a rapid increase in the pressure of both fluids was observed, with the pressure of the nonwetting phase always higher than the pressure of the wetting phase. The front reached the water and PCE sensors at the same time, indicating a relatively homogeneous sand packing. This is an important requirement, as the local phase pressure difference at a given elevation was determined by subtracting the pressure of the nonwetting phase measured on one side of the column from the wetting phase pressure measured on the opposite side. It should be mentioned that no fingering effects were observed as the denser fluid was injected from below and flowed upward.

[22] 4. After a breakthrough of the nonwetting phase to the outflow reservoir, the pressure slowly decreased approaching steady state values.

[23] Figures 2b, 2e, 3b, and 3e show the change of water saturation with time. The change in water saturation was as expected: it decreased rapidly as the PCE front reached a sensor and then leveled off as soon as it passed. It is evident that the higher the injection pressure, the faster the saturation change (reduction) was, and it also approached a lower saturation plateau. It must be noted that after 3 h of injection, steady state was not reached; saturation was still decreasing albeit very slowly.

[24] Plots of fluids pressure differences are shown in Figures 2c, 2f, 3c, and 3f. Except for the 20 kPa experiment, we see a nonmonotonous variation with time. There is an initial sharp increase of the pressure difference to an overshoot and then it decreases to an asymptotic value. We note that the magnitude of this overshoot increases with the increasing of the injecting pressure. This overshoot was not observed in the case of 20 kPa; apparently this injection pressure was not high enough to cause such a nonequilibrium effect. This fact (i.e., the absence of overshoot at lower injection pressure) also implies that the overshoot is not an artifact of the measurement system. In particular, it is not because of a delay in the pressure sensor response. In all experiments, both nonwetting and wetting sensors responded immediately at the change of pressure because of the PCE front advancing along the column. We did some preliminary tests and established that as soon as the PCE front arrived at

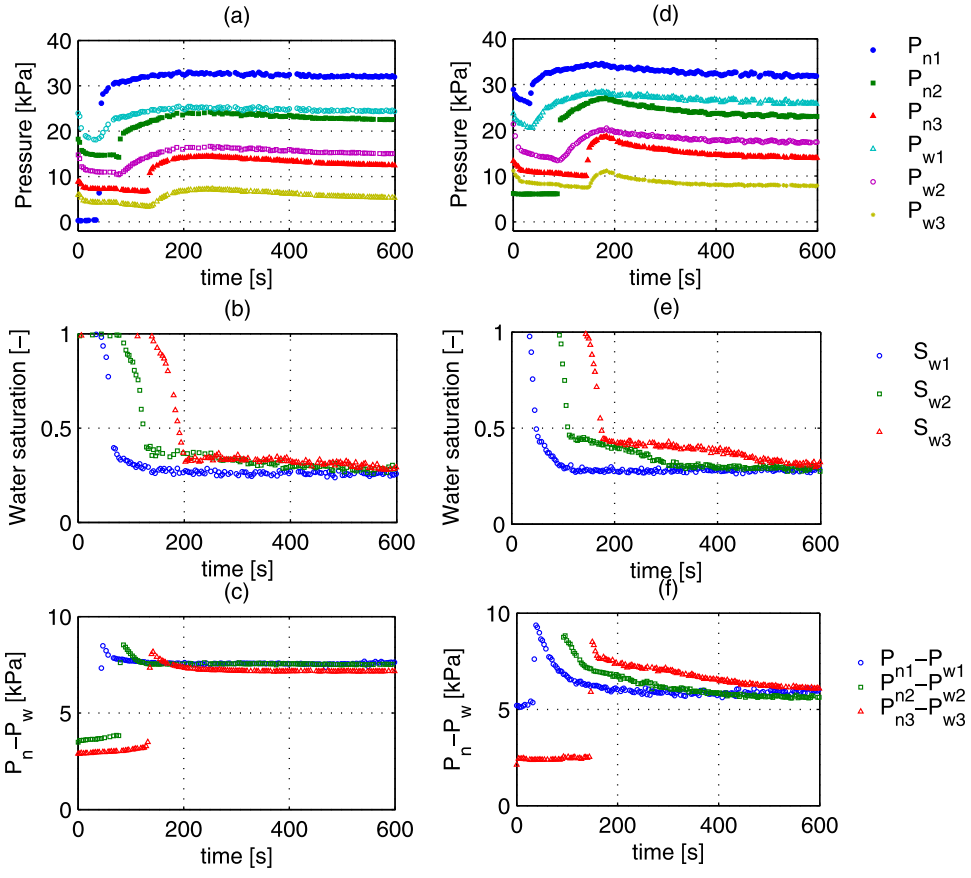

Figure 3. Results of nonequilibrium experiments at three different elevations. Figures on left are at an injection pressure of 35 kPa and right figures are at an injection pressure of 38 kPa. (a) and (d) Wetting and nonwetting phase pressures versus time. (b) and (e) Local water saturation versus time. (c) and (f) Local fluids pressure difference versus time.

a pressure transducer, it responded immediately and the reading corresponds properly to the expected pressure.

[25] Finally, for the four primary drainage experiments, plots of local fluids pressure differences versus local water saturation at elevation z_1 (7 cm) are shown in Figure 4. In the same figure, the local capillary pressure saturation curve is plotted too. This curve was previously determined in equilibrium experiments fully described by *Bottero et al.* [2011]. It is evident that the fluids pressure difference curves lie higher than the capillary pressure saturation curve. This is in agreement with the theory in equation (7). The differences are larger for the larger injection pressures. For the case of primary drainage performed at 20 kPa, the capillary pressure increased monotonously with the decrease of water saturation. A different behavior, however, is seen for experiments performed at higher injection pressures; the fluids pressure difference showed a nonmonotonic trend (an overshoot) at all elevations (z_1, z_2, z_3). Moreover, for higher injection pressures, a larger overshoot is observed. A pressure difference overshoot was also found by *Hassanizadeh et al.* [2004] in drainage experiments on a small sand column, 6 cm in diameter and 3 cm high. The fluid pressures (water-PCE) were measured by transducers installed at the side of the column. Such a nonmonotonic pressure difference behavior is a very significant phenomenon because it cannot be modeled with the standard capillary pressure formula used in the current two-phase flow models. Indeed, *Berentsen et al.* [2006] simulated these drainage experiments and found that the pressure difference overshoot was reproducible only through the inclusion of the nonequilibrium term in

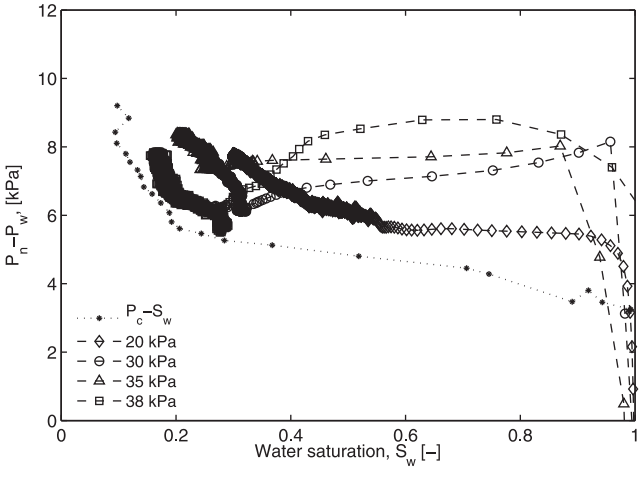

Figure 4. Local fluids pressure difference-saturation curves at injection pressures of 20, 30, 35, and 38 kPa, at elevation z_1. $P_c - S_w$ is also shown.

the governing equations, as suggested in equation (7). The same conclusions were found in numerical simulations by *Bottero* [2009].

[26] *Camps-Roach et al.* [2010] carried out a series of nonequilibrium experiments in a water-air system in a homogeneous fine sand column (entry pressure $P_d = 4.6$ kPa), comparable with the length scale of our column ($h = 20$ cm), where phase pressures were locally measured by means of tensiometers. They did not observe any nonmonotonic behavior in the pressure difference. We find that this is because the injection pressures, compared to the entry, were not high enough to cause nonmonotonic behavior. Their applied pressures were 13 and 21 kPa, therefore the effective pressure gradients, $(P_{\text{applied}} - P_d)/h$, were smaller or equal to the pressure gradients for the lowest injection pressures in our experiments. We also did not observe nonmonotonic behavior at a pressure of 20 kPa.

[27] *Sakaki et al.* [2010] also performed nonequilibrium drainage experiments in an air-water system. They applied a boundary pressure of 12 kPa over a 10 cm sand column (entry pressure $P_d = 3.6$ kPa). Thus, the effective pressure gradient was comparable with the effective pressures gradient applied in our experiment with an injection pressure of 20 kPa. They also found a dynamic effect (i.e., the pressure difference was higher than the capillary pressure) but, they did not observe any nonmonotonic behavior. This is in line with our observations.

4. The Nonequilibrium Coefficient τ at the Local Scale

[28] Experimental data presented in Figures 2 and 3, and plots of $P_n - P_w$ versus S_w in Figure 4, are used to determine the values of the nonequilibrium coefficient τ. According to equation (7), τ is the slope of the curve when $(P_n - P_w) - P_c$ is plotted versus $\partial S_w/\partial t$. For this calculation, we need to have capillary pressure, pressure difference, and the rate of change of saturation, all at a specific saturation for a given elevation. For these calculations, first, the local capillary pressure saturation data points at a given elevation, measured previously by *Bottero et al.* [2011], were fitted by the van Genuchten model [*van Genuchten*, 1980]. This model was preferred to a Brooks-Corey model [*Brooks and Corey*, 1964] as it provided a better fit of the data. Second, the pressure difference $P_n - P_w$ at a specific saturation was calculated by linear interpolation between two data points. Next, from the $S_w - t$ curves at the given elevation, shown in Figures 2 and 3, values of $\partial S_w/\partial t$ were calculated using a central difference scheme. This could not be calculated near low water saturations when the change in saturation was lower than the resolution of TDR system (0.5%). As expected, the largest rate of change of saturation was found at higher injection pressures; the absolute values were 4×10^{-2} [s^{-1}], 2.7×10^{-2} [s^{-1}], 2.2×10^{-2} [s^{-1}] and 1.4×10^{-2} [s^{-1}] at 38, 35, 30, and 20 kPa, respectively.

[29] For each injection pressure, at any given water saturation, $\partial S_w/\partial t$ and $(P_n - P_w) - P_c$ were substituted in equation (7). The resulting τ values are plotted versus water saturation in Figure 5.

[30] An alternative procedure to calculate τ was suggested by *Hassanizadeh et al.* [2004], *Manthey et al.* [2005], and *Manthey* [2006]. At a given saturation, values of $(P_n - P_w) - P_c$ and $\partial S_w/\partial t$ are calculated for each injection pressure. Because we had four different injection pressures, this procedure provides four data points at any given saturation for each injection pressure. If we assume that when $\partial S_w/\partial t = 0$, then the fluids pressure difference should be equal to the capillary pressure (i.e., $[P_n - P_w] - P_c = 0$), and we get a fifth data point. These five data points are fitted by a regression line. The fitting was optimized by applying a least squares Marquardt-Levenberg algorithm, with $\partial S_w/\partial t$ as the independent variable and $(P_n - P_w) - P_c$ as the dependent variable. The slope of the resulting regression line is an estimate of τ at the corresponding saturation. The regression at any given saturation goes through the origin, indicating that the linear relationship between $(P_n - P_w) - P_c$ and $\partial S_w/\partial t$, as in equation (7), is valid. The value of τ calculated following this procedure is plotted in Figure 5 together with the τ values calculated from individual injection pressure. The two methods provided the same τ values within the measurements error, except for one point related to 20 kPa.

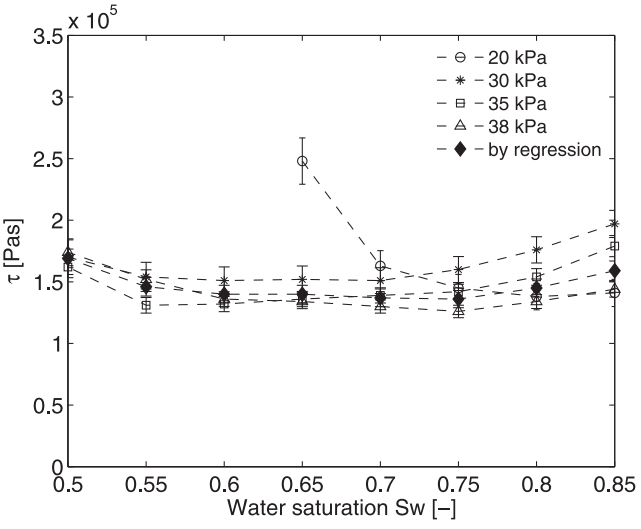

Figure 5. The dynamic coefficient τ versus local water saturation for four different injection pressures. The τ coefficient calculated combining data from all four injection pressures and regressing is also shown.

[31] Except for the lower injection pressure of 20 kPa, which yielded a larger value (2.5×10^5 Pa s), the value of τ does not vary much and one may conclude that it does not depend on the injection pressure. This is in agreement with the finding of *Sakaki et al.* [2010] and *Camps-Roach et al.* [2010] from experiments carried out in an water-air system. For injection pressures of 30, 35, and 38 kPa the damping coefficient varies between 1.35×10^5 and 2×10^5 Pa s. Similar values for τ were found in a series of primary drainage experiments with the same soil type by *Hassanizadeh et al.* [2004], where the estimated values of τ varied between 0.65×10^5 and 1.44×10^5 Pa s. Some lager values were found by *O'Carroll et al.* [2005] who performed multistep outflow (MSO) experiments involving the displacement of water by PCE in an homogeneous sand column 9.62 cm high. In those experiments, fluid pressures were measured in inflow and outside reservoirs only. Column-scale average saturation was

determined from the measurement of accumulated outflow volume as a function of time. Therefore, the coefficient τ could not be determined directly, but it was estimated by inverse modeling fitting the measured outflow volume. They estimated τ to vary between 10^6 to 2×10^6 Pa s. These should be seen as local-scale values because they were assigned to grid cells of their modeling domain. These values are about one order of magnitude larger that the values obtained in our experiments. One reason could be related to the difference in the sand type used. *Stauffer* [1978] suggested that the dynamic coefficient τ should be inversely proportional to the intrinsic permeability. This was also shown experimentally by *Camps-Roach et al.* [2010] who found a larger dynamic coefficient for finer sand. However, the sand used by *O'Carroll et al.* [2005] experiments was coarser ($d_{50} = 0.26$ mm) than the sand used in our experiment. Therefore, the grain size difference cannot justify the discrepancy between the magnitude of τ values. The reason for this discrepancy is not clear to us.

[32] Experimental studies [*Bottero et al.*, 2006; *Chen*, 2006; *Sakaki et al.*, 2010] and computational work [*Manthey et al.*, 2005; *Das et al.*, 2007; *Mirzaei and Das*, 2007; *Gielen*, 2007; *Joekar-Niasar et al.*, 2010] reported in the literature showed that the value of τ is a function of saturation. *Joekar-Niasar and Hassanizadeh* [2010] investigated the effect of the viscosity ratio $M = \mu_{nw}/\mu_w$, on the dynamic coefficient-saturation relationship with a pore network model. For high viscosity ratio, M = 10, similar to the viscosity ratio in our experiments, they found that τ coefficient increases with the decrease of the wetting saturation. In our experiments, as shown in Figure 5, there is no clear dependency of the dynamic coefficient on the water saturation. It must be noted that in our case the dynamic coefficient was not calculated over the entire range of saturation.

5. The Average Nonequilibrium Fluids Pressure Difference

[33] In this section, measured local fluid pressures and saturations are used to calculate average phase pressures and saturations over average windows of 11 and 18 cm. A similar approach was adopted by *Bottero et al.* [2011] to determine an upscaled capillary pressure saturation curve.

[34] The traditional way of averaging pressure is the *intrinsic phase average*, where basically the pressure of the phase is weighed by its saturation. *Nordbotten et al.* [2008] showed that this operator may not be the correct manner of averaging pressure as it leads to a nonphysical extra term in Darcy's law. They introduced another averaging operator, the *centroid-corrected phase average* $[P_\alpha]$, which in one-dimensional form may be written as

$$[P_\alpha] = < P_\alpha > + \frac{1}{\frac{\partial}{\partial z} < z_\alpha >} (\bar{z} - < z_\alpha >) \frac{\partial}{\partial z} < P_\alpha >, \qquad (8)$$

where $< P_\alpha >$ is the intrinsic phase-average pressure, and $\bar{z}$ is the centroid of the averaging volume to which $[P_\alpha]$ is assigned, and it is defined as

$$\bar{z} = \frac{1}{2} H, \qquad (9)$$

where H is the length of the averaging domain. In equation (8), $< z_\alpha >$ denotes the centroid of the domain occupied by phase α, defined as

$$< z_\alpha > = \frac{\sum_{i=1}^{N} S_\alpha^i z^i}{\sum_{i=1}^{N} S_\alpha^i}, \qquad (10)$$

where z^i is the position of the local measurement point i. Basically, this averaging operator corrects the *intrinsic-phase average* pressure $< P_\alpha >$ for the distance between the centroid of the averaging volume, $\bar{z}$, and the centroid of the phase, $< z_\alpha >$. It must be noted that this is a first-order correction, and, as will be discussed later, it is not necessarily valid at high saturations. The derivatives of the *intrinsic-phase average* pressure and the α- phase centroid $< z_\alpha >$, needed in equation (8), can be calculated for a vertical column with upward flow as follows [*Korteland et al.*, 2009]:

$$\frac{\partial}{\partial z} < P_\alpha > = \frac{1}{< S_\alpha > H} \left[- < P_\alpha > \left(S_\alpha^{\text{top}} - S_\alpha^{\text{bot}} \right) + \left(S_\alpha^{\text{top}} P_\alpha^{\text{top}} - S_\alpha^{\text{bot}} P_\alpha^{\text{bot}} \right) \right], \qquad (11)$$

$$\frac{\partial}{\partial z} < z_\alpha > = \frac{1}{< S_\alpha > H} \left[- < z_\alpha > \left(S_\alpha^{\text{top}} - S_\alpha^{\text{bot}} \right) + \left(S_\alpha^{\text{top}} z^{\text{top}} - S_\alpha^{\text{bot}} z^{\text{bot}} \right) \right], \qquad (12)$$

where the subscripts top and bot refer to the values of the variable at the top and bottom boundaries of the averaging domain.

[35] The average saturation is determined simply as the arithmetic average of local saturations:

$$< S_\alpha > = \frac{\sum_{i=1}^{N} S_\alpha^i}{N}. \qquad (13)$$

[36] We performed the averaging over two scales. The smaller averaging window was between $z_1 = 7$ cm and $z_3 = 18$ cm. For this window, the observation points are located at elevations z_1, z_2, and z_3. For the larger domain (18 cm) an extra observation point was considered to be at the bottom of the column, at z_0. The nonwetting phase pressure at elevation z_0 was assumed to be the same as the injection pressure $P_{n0} = P_{\text{bot}}$. The injection pressures employed in our experiments were high enough to displace water from the bottom of the column. So, we assumed that the water saturation at z_0 reached residual saturation already from the very beginning. Another assumption was that the residual saturation and the corresponding $P_n - P_w$ at elevation z_0 were the same as the values for other elevations at the end of each nonequilibrium experiment, which can be read in Figures 2c, 2f, 3c, and 3f. In this way, the local water pressure P_{w0} was determined. Moreover, when the nonwetting phase was not yet present at a given observation point, its pressure was assumed to be the same as that of the wetting phase.

[37] Results from the averaging procedure are shown in Figures 6a–6d. In these figures, the fluids pressure differences for both average windows of 11 and 18 cm are plotted versus the average water saturation. Also, the average capillary pressure obtained by *centroid-corrected* operator from equilibrium experiments [*Bottero*, 2009; *Bottero et al.*, 2011] is plotted versus the average water saturation (solid circles). The curve that goes through data points is obtained by fitting the van Genuchten formula to these data points $(n = 8713, \alpha = 2.079 \times 10^4, R^2 = 099)$. We have also plotted the local fluids pressure difference curve at elevation z_1 for reference (open circles).

[38] It is clear that the average curves of fluids pressure difference lie higher than the average capillary pressure curve. This means that we have a nonequilibrium capillarity effect at the column scale too. Moreover, the average curves show a nonmonotonic behavior, which is typical of nonequilibrium effects. For the average window of 11 cm, the average pressure differences are close to the local ones. It should be noted that larger pressure differences would have been obtained if we had used the *intrinsic volume phase* average operator. During primary drainage, this operator weights high nonwetting pressure values with high nonwetting saturation, whereas high values of the wetting phase pressure are weighted by low saturation. This results in an artificially high value of the pressure difference. As discussed by *Korteland et al.* [2009], *Bottero* [2009], and *Bottero et al.* [2011] it seems that the use of this operator results in a pseudo nonequilibrium effect even under an equilibrium condition.

[39] It should be noted that the *centroid-corrected* pressure difference curves fall below the local-scale curve at high saturations; ~0.8 for the 20 kPa case and 0.9 for the 30 kPa case. This is perhaps an indicator of the approximate nature of the *centroid-corrected* average operator at high saturations [*Korteland et al.*, 2009].

6. Upscaled Damping Coefficient

[40] An open question is whether the value of coefficient τ should vary with the length scale. In section 4, the procedure for calculating the nonequilibrium capillarity coefficient based on the local-scale phase pressures and saturation was presented. The same method was used to estimate the dynamic coefficient at the average window sizes of 11 and 18 cm. For this purpose, curves of average fluids pressure difference and average capillary pressure shown in Figures 6a–6d are used to calculate values of $(P_n) - (P_w) - (P_c)$, at various average saturations.

[41] From local saturations shown in Figures 2 and 3, average saturation $< S_w >$ for the four different drainage experiments (with different injection pressures) were calculated. Then, a centered-difference scheme was used to obtain the average rate of change of saturation. For each injection pressure, at a given saturation, the average values were substituted in equation (7). The resulting average coefficient is denoted by $[\tau]$.

[42] The average nonequilibrium coefficient for each injection pressure, for both averaging windows, are plotted in Figure 7 versus water saturation, where error-bars are also shown. The larger errors at the averaged scale compared to points values, are because of error propagation in the calculation of average pressures and saturations. It is still

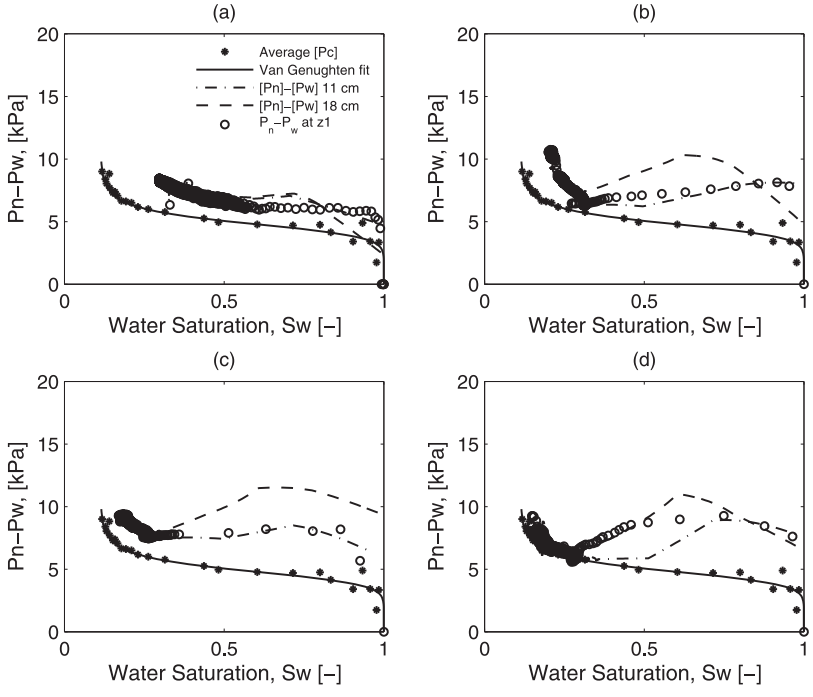

Figure 6. Average fluid pressure differences plotted versus average wetting phase saturation at the length scales of (dotted-dashed lines) 11 cm and (dashed line) 18 cm for four different injection pressures: (a) 20 kPa, (b) 30 kPa, (c) 35 kPa, and (d) 38 kPa. (Open circles) The corresponding local data points at elevation z_1. (Solid circles) The average capillary pressure saturation data points, and (solid line) the van Genuchten curve fitted to the average $P_c - S_w$ points are also shown.

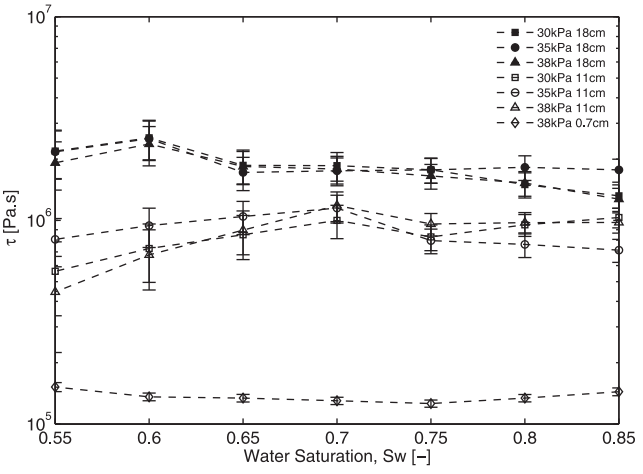

Figure 7. Average dynamic coefficients $[\tau]$ at the length scales of 11 and 18 cm for different injection pressures. The local nonequilibrium coefficient τ at the scale of 0.7 cm is also reported for reference. The vertical axis is in logarithmic scale.

clear that the value of average nonequilibrium coefficient increases with the increase of the length scale. At the average window of 11 cm, $[\tau]$ was found to vary between 0.5×10^6 and 2×10^6 Pa s which are one order of magnitude larger than the local τ values (sensor scale of 0.7 cm). Even larger values were found for the length scale of 18 cm, where minimum and maximum were 1.4×10^6 and 2.3×10^6 Pa s, respectively. However, it must be noted that τ value does not scale with the square of length, such a dependence was suggested by *Dahle et al.* [2005] based on results of a bundle of tubes model.

[43] As shown in Figure 6, the magnitudes of the pressure difference at the local scale (0.7 cm) and 11-cm scale are close to each other. Therefore, the scale dependency of the dynamic coefficient is mainly because of the rate of change of saturation, whose magnitude decreases with the increase of the length scale. For example, at an injection pressure of 35 kPa at $S_w = 0.70$, the rate of change of saturation was found to be $|4 \times 10^{-2}|[s^1]$ at local scale and $|4 \times 10^{-3}|[s^{-1}]$ at the scale length of 11 cm.

[44] Dependency of the nonequilibrium coefficient on the length scale has been reported in numerical studies by *Manthey et al.* [2005] and in a pore scale modeling by *Dahle et al.* [2005]. *Manthey et al.* [2005] simulated the displacement of water by PCE in a homogeneous coarse sand and considered four domain sizes varying from 0.03 to 1 m. The pressure gradient across the domain was kept the same in all simulations. They found the average τ value to be larger for larger domains, scaling with the square of domain size. Similar results were found by *Dahle et al.* [2005]. Such scale-dependence is not uncommon in the physics of porous media. For example, dispersivity is also known to increase with the length scale of observation [*Bear*, 1972].

[45] However, such a scale-dependence was not found by *Camps-Roach et al.* [2010] from experiments preformed in a homogeneous porous media for a water-air system. The local pressures and saturations at the sensor scale of 1 cm were averaged over two different domain sizes, namely 6 and 9 cm. Even though they used the *intrinsic phase-average* operator to obtain average pressures, they found no difference in the magnitude of the pressure differences between local and average scale. Moreover, they found that the magnitude of the desaturation rate at local scale (sensor scale 1cm) was the same as the values for larger domain sizes. Therefore, the magnitude of τ did not vary with the average window. For the fine sand they found τ values ranging between 10^5 and 10^6 Pa s at both local and average scales.

[46] *O'Carroll et al.* [2005] also calculated the value of $< \tau >$ representative for their whole domain (9.62 cm). The average fluids pressure difference was assumed to be calculated by subtracting the water pressure measured at the top reservoir from the nonwetting phase pressure imposed at the bottom of the column. The rate of change of saturation was calculated on the basis of the average water saturation at the end of the outflow step at an effective saturation of 0.50. They found a dynamic coefficient of $\tau = 2.8 \times 10^7$ Pa s, which is comparable with their local value of $\tau = 1.63 \times 10^7$ Pa s. Obviously, there is no consensus on the scale-dependence of τ coefficient and more investigations are needed.

7. Summary and Conclusions

[47] A series of primary drainage experiments were carried out in order to investigate the nonequilibrium capillary effect in two-phase flow through porous media. Our experimental results showed that throughout the nonequilibrium process, the fluids pressure difference-saturation curves lay higher than the capillary pressure saturation curve. Moreover, the nonequilibrium pressure difference showed a nonmonotonic behavior, i.e., an overshoot, which was more pronounced at higher injection pressures.

[48] Based on measured local pressures and saturations, average fluid pressures and saturations were calculated for the length scales of 11 and 18 cm. The *centroid-corrected* average operator was used to determine average phase pressures. It was found that the average nonequilibrium pressure difference, based on the *centroid-corrected* averaging operator, lay above the average capillary pressure, and it showed a nonmonotonic behavior.

[49] We used the measured data to calculate local-scale values of the damping coefficient τ. We did not find a clear dependency of this coefficient on saturation, for the saturation range of 0.5 to 0.85. Its values at the local scale (0.7 cm) were found to vary between 1.3×10^5 and 2×10^5 Pa s. Also, no dependence of the dynamic coefficient on the injection boundary pressure was found. Thus, our results show that in the saturation range $0.50 > S_w > 0.85$, there is a linear relationship between $P_n - P_w - P_c$ and the rate of change of saturation.

[50] The average values of the dynamic coefficient were calculated for two different averaging domain sizes. The nonequilibrium capillarity coefficient was found to vary between 0.5×10^6 and 1.2×10^6 Pa s at the length scale of 11 cm. Larger values were found at the length scale of 18 cm: $1.5 \times 10^6 - 2.5 \times 10^6$ Pa s. This suggests that the dynamic coefficient is scale dependent.

[51] **Acknowledgments.** This research was supported by Utrecht Center of Geoscience (UCG). The authors would like to thank Tohren Kibbey and Denis O'Carroll for their comprehensive and constructive review of the manuscript, their comments helped to improve the manuscript.

References

Bear, J. (1972), *Dynamics of Fluids in Porous Media*, 2nd ed., 784 pp., Dover Publ., N. Y.

Berentsen, C. W. J., S. M. Hassanizadeh, A. Bezuijen, and O. Oung (2006), Modelling of two-phase flow in porous media including non-equilibrium capillary pressure effects, Proceeding XVI International Conference on Computational Methods in Water Resources, Tech. Univ. of Denmark, Copenhagen, Denmark.

Bottero, S. (2009), Advances in the theory of capillarity in porous media, Ph.D. thesis, Geologica Ultreietina, *314*, 200 pp.

Bottero, S., S. M. Hassanizadeh, P. J. Kleingeld, and A. Bezuijen (2006), Experimental study of dynamic capillary pressure effect in two-phase flow in porous media, Proceedings of the XVI International Conference on Computational methods in Water Resources, Tech. Univ. of Denmark, Copenhagen, Denmark.

Bottero, S., S. M. Hassanizadeh, and P. J. Kleingeld (2011), From local measurements to an upscaled capillary pressure-saturation curve, *Transp. Porous Media*, doi:10.1007/s11242-011-09739-4.

Brooks, R. H., and A. T. Corey (1964), Hydraulic properties of porous media, Hydrology paper, Colorado State University, CO.

Camps-Roach, G., D. M. O'Carroll, T. A. Newson, T. Sakaki, and T. H. Illangasekare (2010), Experimental investigation of dynamic effects in capillary pressure: Grain size and upscaling, *Water Resour. Res.*, *46*, W08544, doi:10.1029/2009WR008881.

Chen, L. (2006), Hysteresis and dynamic effects in the relationship between capillary pressure, saturation, and air-water interfacial area in porous media, Ph.D. thesis, University of Oklahoma, OK.

Dahle, H. K., M. A. Celia, and S. M. Hassanizadeh (2005), Bundle-of tubes model for calculating dynamic effects in the capillary-pressure-saturation relationship, *Transp. Porous Media*, *58*, 5–22.

Das, B. D., R. Gauldie, and Mirzaei, M. (2007), Dynamic effects for two-phase flow in porous media: Fluid property effects, *AIChE*, *53*(10), 2505–2520.

Gielen, T. W. J. (2007), Upscaling multiphase transport processes in porous media, Ph.D. thesis, Delft University of Technology, Netherlands.

Hassanizadeh, S. M., and W. G. Gray (1990), Mechanics and thermodynamics of multiphase flow in porous media, *Adv. Water Resour.*, *13*, 169–186.

Hassanizadeh, S. M., and W. G. Gray (1993), Thermodynamic basis of capillary pressure in porous media, *Water Resour. Res.*, *29*, 3389–3405, doi:10.1029/93WR01495.

Hassanizadeh, S. M., M. A. Celia, and H. K. Dahle (2002), Dynamic effect in the capillary pressure-saturation relationship and its impact on unsaturated, *Vadose Zone Hydrology*, *1*, 38–57.

Hassanizadeh, S. M., O. Oung, and S. Manthey (2004), Laboratory experiments and simulations on the significance of the non-equilibrium effect in capillary pressure saturation relationship, in *Unsaturated Soil: Experimental Studies: Proceedings of the International Conference: From experimental evidence towards numerical modeling of unsaturated soils*, Weimar, Germany, *1*, 3–14.

Helmig, R. (1997), Multiphase flow and transport processes in the subsurface: A contribution to the modeling of hydrosystems, 279 pp., Springer, Berlin, Germany.

Joekar-Niassar, V., and S. M. Hassanizadeh (2010), Effect of fluids properties on non-equilibrium capillarity effects: Dynamic pore-network modeling, *Int. J. Multiphase Flow*, doi:10.1016/J.iJmultiphaseflow.2010.09.007.

Joekar-Niassar, V., and S. M. Hassanizadeh (2011), Dynamics of two-phase flow in porous media; from pore scale to darcy scale (a review), *Critical Rev. Env. Sci. Tech.*

Joekar-Niassar, V., S. M. Hassanizadeh, and H. K. Dahle (2010), Non-equilibrium effects in capillarity and interfacial area in two-phase flow: Dynamic pore-network modelling, *J. Fluid. Mech.*, *655*, 38–71, doi:10.1017/S0022112010000704.

Kalaydjian, F. (1992), Dynamic capillary pressure curve for water/oil displacement in porous media, theory vs. experiments, Proc. SPE Conference, Washington DC. SPE, Brookfield, CT., *SPE 24813*, 491–506.

Korteland, S., S. Bottero, S. M. Hassanizadeh, and C. W. J. Berentsen (2009), What is the correct definition of average pressure?, *Transp. Porous Media*, doi:10.1007/s11242-009-9490-2.

Malicki, M. A., R. Plagge, and C. H. Roth (1994), Influence of matrix on TDR soil moisture readings and its elimination., Proc. of the Symp. on Time Domain Reflectometry in Environmental, Infrastructure, and Mining Applications, Evaston, IL, Sept. 7–9, U.S. Bureau of Mines, Spec. Publ. SP 19-94, NTIS PB95-105789, pp. 105–114.

Manthey, S. (2006), Two-phase flow processes with dynamic effects in porous media-parameter estimation and simulation, Ph.D. thesis, University of Stuttgart, Stuttgart, Germany.

Manthey, S., S. M. Hassanizadeh, and R. Helmig (2005), Macro-scale dynamic effects in homogeneous and heterogeneous porous media, *Transp. Porous Media*, *58*, 121–145, doi:10.1007/s11242-004-5472-6.

Mirzaei, M., and D. B. Das (2007), Dynamic effects in capillary pressure-saturation relationships for two-phase flow in 3D porous media: Implication of micro-heterogeneities, *Chem. Eng Sci.*, *62*(7), 1927–1947.

Nordbotten, J. M., M. A. Celia, H. K. Dahle, and S. M. Hassanizadeh (2008), On the definition of macro-scale pressure for multi-phase flow in porous media, *Water Resour. Res.*, *44*, W06S02, doi:10.1029/2006WR005715.

O'Carroll, D. M., T. J. Phelan, and L. M. Abriola (2005), Exploring dynamic effect in capillary pressure in multistep outflow experiments, *Water Resour. Res.*, *41*, W11419, doi:10.1029/2005WR004010.

Oung, O., and A. Bezuijen (2003), Selective pore pressure transducer for use in model tests to study two-phase flow in porous media, *IJPMG-International Journal of Physical Modelling in Geotechnics*, *4*, 31–41.

Sakaki, T., D. M. O'Carroll, and T. H. Illangasekare (2010), Direct quantification of dynamic effects in capillary pressure for drainage-wetting cycles, *Vadose Journal*, *9*, 424–437, doi:10.2136/vzj2009.0105.

Schaap, M. G., L. de Lange, and T. J. Heimovaara (1997), TDR calibration of organic forest floor media, *Soil Technology*, *11*, 205–217.

Sheng, P., and M. Zhou (1992), Immiscible-fluid displacement: Contact-line dynamics and the velocity-dependent capillary pressure, *Phys. Rev.A*, *45*(8), 5694–5708.

Smiles, D. E., G. Vachaud, and M. Vauclin (1971), A test of t he uniqueness of the soil moisture characteristic during transient, nonhysteretic flow in a rigid soil, *Soil Sci. Soc. Amer. Proc.*, *35*, 534–539.

Stauffer, F. (1978), Time dependence of the relations between capillary pressure, water content and conductivity during drainage of porous media, in *On Scale Effects in Porous Media*, Thessaloniki, Greece.

Topp, G. C., A. Klute, and D. B. Peter (1967), Comparison of water content-pressure head obtained by equilibrium, steady-state, and unsteady-state methods, *Soil Sci. Soc. Amer. Proc.*, *31*, 312–314.

Vachaud, G., M. Vauclin, and M. Wakil (1972), A study of the uniqueness of the soil moisture characteristic during desorption by vertical drainage, *Soil Sci. Soc. Amer. Proc.*, *36*, 531–532.

van Genuchten, M. T. (1980), A closed-form equation for predicting the hydraulic conductivity of unsaturated soils, *Soil Sci. Soc. Am. J.*, *44*(5), 273.

Wildenschild, D., J. W. Hopmanns, and J. Simunek (2001), Flow rate dependence of soil hydraulic characteristics, *Soil Sci. Soc. Am. J.*, *65*, 35–48.

S. Bottero, Department of Biotechnology, Delft University of Technology, Julianalaan 67, 2628 BC Delft, Netherlands. (s.bottero@tudelft.nl)

S. M. Hassanizadeh and P. J. Kleingeld, Department of Earth Sciences, Utrecht University, P.O. Box 80021, 3508 TA Utrecht, Netherlands.

T. J. Heimovaara, Geo-Engineering Section, University of Technology, P.O. Box 5048, 2600 GA Delft, Netherlands.